

## Specific Aims

Integrating magnetic resonance imaging (MRI) functionality with radiation therapy (RT) linear accelerator (LINAC) can better render the visualization of the soft tissues of lesions and surrounding healthy organs-at-risks (OARs) during cancer RT treatment planning and procedures. This is because MR scans, in contrast to the prevalent computed tomography (CT) scans used in clinics today, provide a richly contrasted image of internal body tissues. More importantly, MRI-LINAC integration can be done in an unrivaled, online, and real-time fashion to aid a more precise radiation dose delivery in RT [1]. However, the quality of MR scans are limited by head motion artifacts. Given the consistency of head motion requirement for proper beam targeting in stereotactic radiosurgery (SRS) and highly conformal head-and-neck (H&N) RT, rigid head frames or thermoplastic face masks are currently clinically used as static head immobilizers. However, frames are uncomfortable and highly invasive – causing poor patient compliance and clinical inefficacy; and masks reduce dose targeting accuracy – since mask flex can lead to drifts of up to 6 mm from an intended target. Robot mechanisms for real-time head motion correction that have been investigated are made out of linear actuators and rigid metallic components which are incompatible with MR [2–4]. During my PhD, I used soft manipulators for head motion correction in RT treatment planning in lower task space dimensions. Here, we propose a novel non-magnetic and radiation-transparent soft robot for automating the online, real-time patient head motion correction in emerging MRI-linear accelerator (LINAC) RT treatment procedures. Our team, comprised of material mechanics, medical physics, control systems and soft matter experts, will address these issues via the following specific aims:

### **K99 Aim I: To Develop a Distributively-Innervated, Non-magnetic, and Radiation-Transparent Soft Actuator.**

My preliminary soft manipulator designs have been used to control H&N motion in RT for up to 3 DoFs. This aim will scale my previous designs to a fully parallel soft robot capable of providing head manipulation along 6 DoFs and will be integrable with pre-existing LINACs. The actuators will be fiber-reinforced to constrain deformation along specific Eulerian directions in order to simplify control. Made entirely out of radio-transparent and non-metallic parts, this Gen 2.0 design will be adaptable under MR coils and the large tubular MR magnets and hence suitable for patient head motion compensation in emerging MRI-LINAC treatment procedures. A hierarchical sensing and control scheme is proposed: the soft actuators will deform in a manner similar to the fast activation ( $\leq 2$ secs) of, for example, the papillae of the octopus, and will have rich surface innervation (e.g. similar to the cuttlefish skin) to aid rich system state perception; this will enable accurate feedback control of the pressurization within the actuator's air chambers. *We expect that this bleeding-edge application will demonstrate for the first time that soft actuators can excel at precise deformation schemes that are safe and compliant for real-world medical applications.*

### **K99 Aim II: To Develop a Multi-Modal and Robustly Stable Optimal Motion-Planner.**

Our preliminary results show the need for a head manipulation motion planner that is safety-aware for executing optimal collision-free paths between transition modes such that manipulating the patient's head does not expose normal brain tissues to high radiation doses. This aim will find a robustly stable and optimal head motion trajectory for moving the head from a start location  $\xi_i \in SE(3)$  to a goal location  $\xi_f \in SE(3)$  safely. As the desired head motion is continuous with discrete underlying structures, the manipulation problem is multi-modal with a continuous admixture of modes. The current convention in robotics is to use layered planning whereby search is hastened by solving a planning problem at various abstraction levels. However, such planners often miss stability-guarantees in their optimal path formulations hence resulting in paths that are not stably robust for assuring safety in the execution of planned paths. *We will address the current gap in geometric manipulation problems under manifold constraints that leave out stability analysis by leveraging an asymptotically stable robust control Lyapunov function optimally stable motion-planning feedback controller in order to safely generate optimally-robust single modes that guide transitions that precisely move the head in the presence of medical constraints in the head-robot workspace.*

### **K99 Aim III: Mechanism Assembly, Phantom, and Healthy Volunteer Experiments.**

A soft robot mechanism will be constructed, able to fit under the MR coils and able to (re)position the patient as needed during treatment. In addition, a 3D surface imaging sensor will measure patient's head position and feed it to the motion planner's head position feedback controller. Patient safety systems based on automated treatment beam shut off will be incorporated into the finished design. The motion-planner in K99 Aim II will be used in the real-time head motion correction in mock MRI-LINAC RT phantom and healthy human volunteer experiments. An end-to-end testing with 3D-printed head phantoms containing dosimetric gel will be used to evaluate 3D radiation dose accuracy for both single and multiple target SRS plans. A 20 volunteer study with a mock radiation beam will be conducted in a clinical environment to verify linear and angular head position control and patient safety systems.

### **R00 Aim: Patient Oncological Clinical Trials.**

A clinical trial on 20 whole brain patients will be performed where validation of this system will be determined by a statistical endpoint. Success will be that a 6D intracranial target is  $\leq 0.5$ mm and  $\leq 0.5^\circ$  for greater than 95% of the treatment time. Upon successful completion and novel use in maskless MRI-LINAC systems, this project will demonstrate that soft robotic SRS is ready for widespread clinical deployment. With its transformational clinical potential, our soft robot head motion compensation in MRI-LINAC RT will enable the availability of novel radiation dose delivery to a larger population of patients, improve therapeutic outcomes, reduce patient invasiveness, improve clinical efficiencies by reducing current setup times from hours to minutes, and will be compatible with thousands of pre-existing LINACs.

**Future Plans:** I plan to expand this project into my own independent research laboratory where I will study to design and control soft robots for broad biomedical engineering applications in human-robot interfaces.



**for precise MRI-LINAC RT treatment procedures.** Existing frame-based immobilization devices, Fig. 1a&b, and frameless and maskless rigid robotic motion correction mechanisms, Fig. 1c&d, are not suitable for this because of their electro-mechanical parts that introduce serious safety concerns. Furthermore, I hypothesize that an asymptotically stable in the large and optimal motion-planner can find collision-free paths that satisfy head motion constraints can resolve the abnormalities inherent in current controllers used in head motion correction systems [2, 3, 16, 20]. I will test this leading hypothesis to see if 6-DOF target motion of a patient is  $\leq 0.5$  mm and  $\leq 0.5^\circ$  for greater than 95% of the treatment time using MRI imaging for soft robot-based motion compensation.

Along with other experiments where I verified that vision-based control of soft robots can geometrically correct patient motion precisely fast-enough in real-time up to three DOFs [19–22], and existing hybrid MRI-compatible RT systems [5, 9, 10], we will test these hypotheses that soft robots can provide position accuracy that is consistent for use in standalone MRIs, MRI-LINAC RT systems or SRS-alone treatment procedures in order to (i) negate the deleterious effects of *interfractional* setup variation on patients; (ii) correct the complex *intrafractional geometric uncertainties* such as posture changes, and body deformation with minimal invasiveness; (iii) eliminate radiation attenuation associated with the metallic components of frames and rigid robotic patient motion compensation systems; and (iv) correct the flex associated with thermoplastic face masks; while *not interfering with the MR machine's magnetic field*.

### 3.2 Innovation.

Our study is innovative in the following respects:

- my work was the first to demonstrate the feasibility of vision-based 3 DOF control of soft manipulators for cranial motion management in RT [19–22]; we are extending this to 6-DOF control with my novel advanced mechanism;
- this mechanism is made entirely of no metal (hence not susceptible to magnetic fields) and is radiation-transparent so that it is compatible with both MRI-LINACs;
- this mechanism can be adapted to confined spaces under MRI coils (see Fig. 1b) given its compactness, and light weight.
- it possesses little invasiveness to the patient, and
- exhibits a quick-connect, quick-disconnect modularity on a couch – important for patients with varying cranial anatomy – thus easing the logistical setup workload of current immobilization and maskless robotic systems.

To our knowledge, **no currently-available technology exists today that can perform real-time head position stabilization without dose attenuation in an online, real-time fashion whilst guaranteeing patient safety similar to our proposed MRI-LINAC non-magnetic and radio-transparent soft robot RT positioning system.** As photon-based cancer treatment accounts for > 50% of all cancer treatments [26], these exploratory experiments are relevant to public health and have transformational clinical potential because they may provide (i) proof-of-concept evidence that soft robots are compatible with standalone MRI imaging modalities; (ii) evidence of precise and automatic motion management with non-magnetic and radiation-transparent soft robots in emerging hybrid MRI-accelerator RT; (iii) an emergence of a better brain and H&N cancer management technology that can be adapted to confined spaces under MRI coils (see Fig. 1b). Upon successful completion, this soft robot will be used for active head motion stabilization within an MR machine. It will be adaptable for standalone MRIs, emerging MRI-LINAC technologies, and brain as well as H&N RTs. It will provide accurate RT beam targeting as well as preventing patient motion MRI imaging artifacts. This technology will improve therapeutic outcomes, and eliminate patient invasiveness.

### 3.3 Approach.

#### 3.3.1 K<sub>99</sub> Aim I: To Develop a Distributively-Innervated, Non-magnetic, and Radiation-Transparent Soft Actuator.

**Rationale:** For though the design of § 3.1.4 is relevant to head motion control on an RT treatment table, it is not a complete motion correction system owing to its underactuated mechanism: it is only able to correct motion for up to three DoFs. Motion of the head occurs along six DoFs and they are not independent. Therefore, to realize a full patient motion compensation, more actuators are needed in the mechanism. To this end, and iterating further on my previous designs [20–22], I now propose a new class of continuum, compliant and configurable (C3) light, and agile soft actuators [24, 27, 28] which are the composition of a non-magnetic and radiation-transparent soft robot for use in MRI-LINACs to further aid dose delivery precision. The component soft actuators are planar and circular in their reference configuration. Upon compressed air actuation, they deform along the radial direction (see computer model in Fig. 7) based on the physical constraints baked into the elastomer-fabric matrix. This actuation design is inspired by the behavior of the skin papillae of certain Cephalopods (octopus, cuttlefish, bivalves and mollusks) which can transform their physical texture from 2D to 3D in less than 2 seconds [29, 30]. The actuators exhibit a radially symmetric deformation and are constrained along their circumferential axis under pneumatic actuation based on their novel design. There exists no electrical wirings or embedded electronics to assure that the actuators reach a desired configuration.

**Hypothesis:** Based on previous success of air actuated elastomeric chambers for manipulating patient head motion correction in real-time, I hypothesize that a fully-compliant and parallel soft robot can effectively correct patient head motion (given a robustly stable and

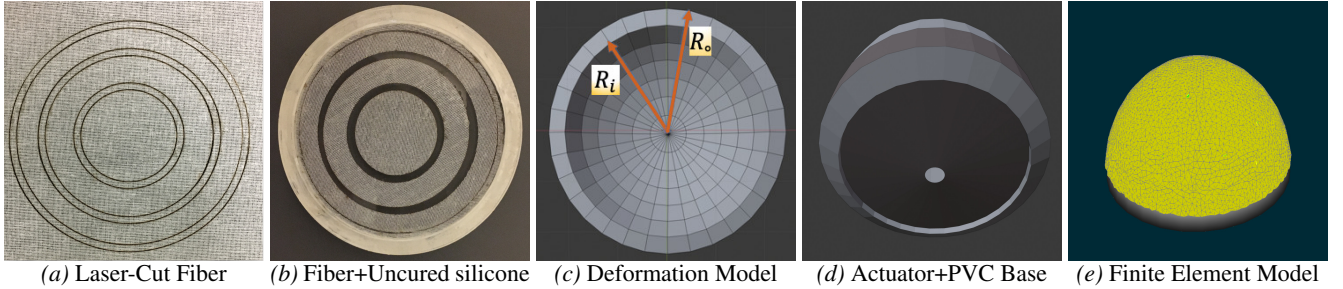


Figure 7: Soft actuator fabrication procedure.

optimal controller) such that the motion artifacts that are prone in MR imaging can be eliminated. This will assure an improved RT treatment outcomes in modern MRI-LINAC RTs.

#### Procedure.

**A. Soft Actuator Design:** The soft actuator fabrication methodology is illustrated in Fig. 7. A thin-layered fabric is laser cut into circular patterns (Fig. 7a), the cut meshes are removed and laid onto uncured silicone (Fig. 7b) which has been poured into mold. We further add a silicone topcoat layer to the fabric before we allow it to cure. Upon low pneumatic pressurization, the cured rubber deforms, obeying a Circumferentially-COnstrained And Radially Stretched fiber-Elastomer (CCOARSE) property [31] (Fig. 7c). This unique deformation pattern is similar to the way a balloon would stretch along its axial direction if a rope were tied around its circumference. The soft robot, after cure, is laid onto an impact-resistant, low-temperature rigid PVC insulation foam sheet, encased in a carbon fiber material. This aids radiation transparency (Fig. 7d). The finite elastic deformation mesh model of the soft robot for simulation purposes is shown in (Fig. 7e). This proposed fabrication method allows us to rapidly iterate different designs using compressed low air pressure (1-15 psi) that is (i) cheaply available, (ii) environmentally-friendly, (iii) avoids electrical wirings, (iv) is lightweight, and (v) inviscid which will make the soft robot adaptable for MRI-LINAC systems – creating a clean and safe human-robot workspace. As the air inflow into the air chambers of the elastomers need to be carefully regulated, we will build current source electronic regulator circuits that proportionally vary the amount of airflow through connecting hoses that lead into the proportional solenoid valves used in earlier experiments [20].

**B. Pneumatic System Design:** We now describe the integration of the soft actuator design proposed above with the rest of the pneumatic actuation system. This system is illustrated in Fig. 8. A self-contained compressed air canister supplies air at a fixed pressure (e.g. 15 psi) through a firm polyurethane air tubing into a 4-20mA output-M12 pressure transducer plug connection. The choice of pressure transmitter is important owing to the accuracy requirement for air volume within the chamber of the soft actuator. In our experience, the G2 series of pressure transducers from Ashcroft® are an excellent choice for such application as this: it offers a  $\pm 1.00\%$  total error band accuracy; being highly configurable, it offers a pressure range that meets our actuation needs and it can be easily integrated into our overall mechanism. The outlet of this pressure transmitter conveys the airflow into a proportional solenoid valve. We use proportioning valves to control the amount of airflow into the actuator’s air chamber because of the air flow precision requirement needed to correctly manipulate the head. The outlet of this solenoid valve then leads to the inlet air connector of the soft actuator. The electronic regulating circuit shown in Fig. 8 is a standard current source circuit that varies the air flow rate within the proportional valve by adjusting the current flowing through its shunt resistor. In addition, a venturi pump removes air at a proportional pressure compared to the inlet supply pressure. This pressure differential helps maintain head along a setpoint or follow a varying trajectory.

**C. Preliminary Actuation Experiments:** We have initial experiments that reproduces deformation behavior similar to the spike observed in the skin papillae of the Octopus. This is described in what follows. We cast silicone from Smooth-On Inc’s dragon skin (475 psi tensile strength and 10A shore hardness), whose material properties exhibit enough softness for patient comfort and enough firmness that withstands extremely nonlinear deformation from the wrench produced by the typical human head (55-65 kg [32–34]). The ingrained fabric membrane within the elastomer imposes the CCOARSE property, constraining the circumferential expansion of the rubber and exerting a radially symmetric stretch as shown in the bottom row of Fig. 9. This considerably simplifies the dynamics model that governs the deformation [28]. Two different designs are shown in the top and bottom rows of Fig. 9. The rubber material is screwed onto a bottom PVC foam sheet using a laser-cut acrylic planar ring. We use **nylon** Phillips screws. The behavior at different levels of pressurization are indicated in each column of the figure. The top row shows the cured silicone without fabric while the bottom row shows the silicone with the entrenched fiber matrix within the elastomer. As can be seen, the material in the top row exhibits a circumferential bulge as well as radial bulge while the ones in the bottom row only extend along the axial direction. As can be seen in the bottom row, we can generate a full *Gaussian deformation* and return to the reference planar configuration in 2 seconds (see more images and videos in [scriptedonachip.com/soro](http://scriptedonachip.com/soro)) similar to the spikes produced by the skin papillae of the Octopus. These quick Gaussian spikes will be useful for rapid head motion correction in MRI-LINACs. The soft compliance and tensile strength of this silicone material make it well-suited for treatment procedures where non-magnetic and radiation-transparent components can boost stereotactic precision as well as improve tumor control in MRI-LINACs.

**D. Flexible Piezoresistive Distributed Sensor Integration:** In a recent formulation [24], we mapped the relationship between the

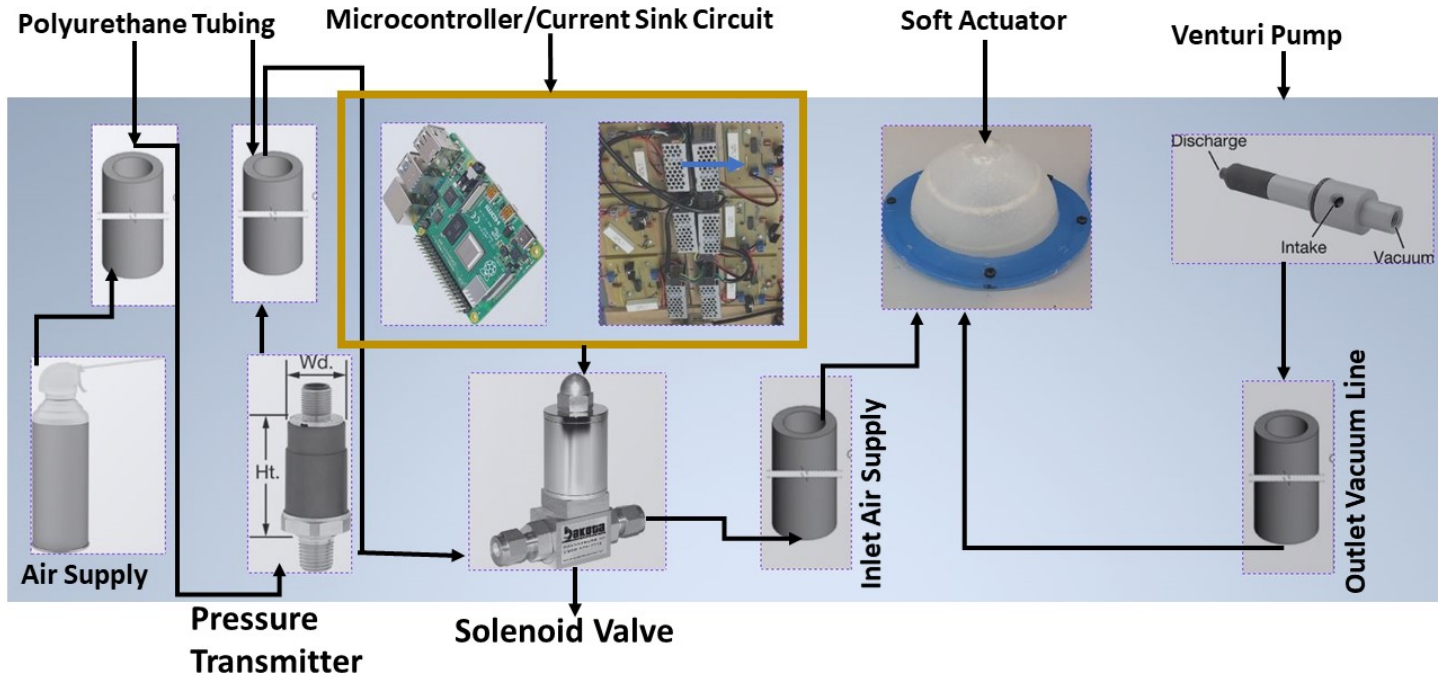


Figure 8: Pneumatic System showing proportional solenoid valve, electronic pressure regulators and raspberry pi microcontroller.

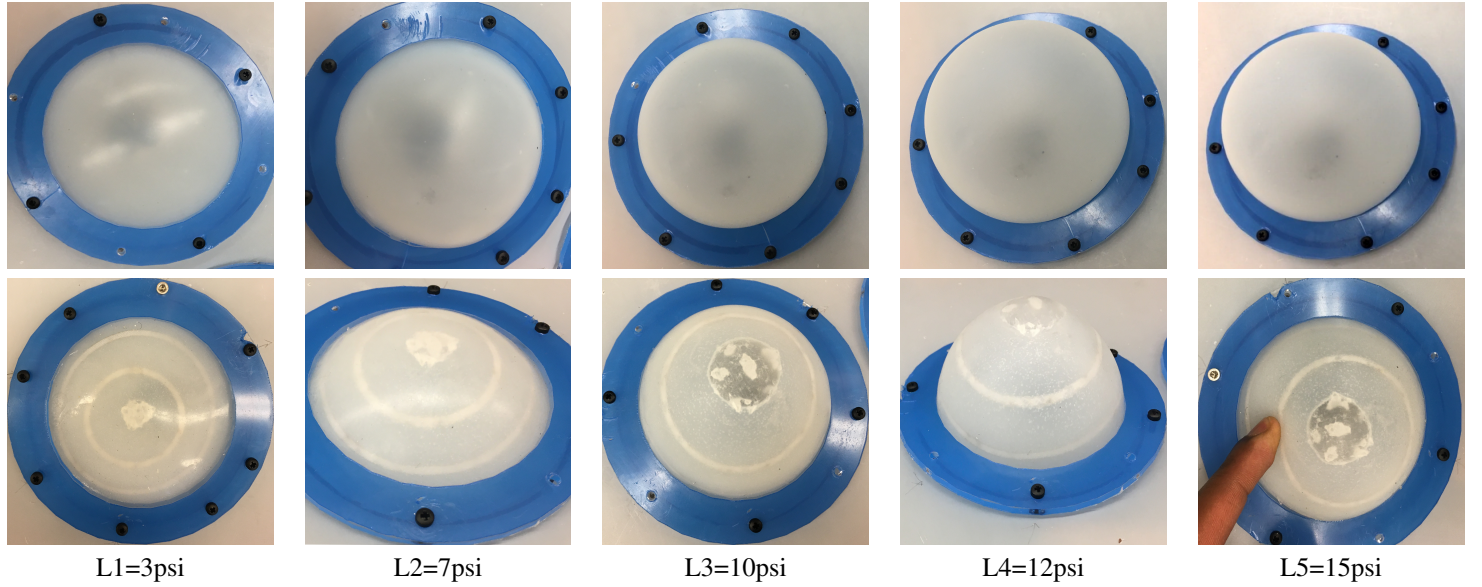


Figure 9: Deformation Levels of elastomer (top) and Elastomeric-Fiber Matrix (bottom) under Low Air Pressurization (3-15psi).

applied pressure to the deformed radius of a soft actuator using the standard Mooney-Rivlin formulation [35, 36]. Suppose that  $C_1$  and  $C_2$  are appropriate material moduli for the soft actuator, then the applied pressure in the internal walls of the actuator is given by the relation

$$P(r) = \int_{r_i}^{r_o} \left[ 2C_1 \left( \frac{r}{R^2} - \frac{R^4}{r^5} \right) + 2C_2 \left( \frac{r^3}{R^4} - \frac{R^2}{r^3} \right) \right] dr \quad (1)$$

where  $r_i$  and  $r_o$  are respectively the internal and external radius of the actuator walls in the current configuration, and they have



control law that yields the path  $c$ , the pointwise min-norm control law yields a robustly stabilizable and optimal synthesis of the head motion correction problem.

**C. Manifold Constraints:** It is not enough for us to find a valid path  $c$  that is free of collisions. We also want the head motion to follow constraints that are functions of the robot's geometry, avoids radiation hitting critical structures, follows a path that does not increase proneness to claustrophobia [62], and lower the problem's dimensionality. Similar to [60], we define these *manifold constraints* to capture loop closure constraints, end-effector constraints etc. A forward kinematic map from the configuration of the  $i^{th}$  IAB,  $\chi_{iab_i}$ , maps from respective IAB configurations to head position and orientation *i.e.*  $K_{iab_i} : \chi_{iab_i} \rightarrow SE(3)$ . The head velocity with respect to a fixed base frame in terms of IAB velocities can be written in terms of the forward kinematics Jacobian:

$$\begin{pmatrix} v_{iab_i} \\ \omega_{iab_i} \end{pmatrix} = \frac{\partial K_{iab_i}}{\partial \mathbf{r}_i} \frac{d\mathbf{r}}{dt} K_{iab_i}^{-1} = \mathbf{J}_i(\mathbf{r}_i) \dot{\mathbf{r}}_i \quad (4)$$

where  $\mathbf{r}_i$  is the spatial position of IAB  $i$  in generalized coordinates, and  $(v_{iab_i}^T, \omega_{iab_i}^T) \in \mathbb{R}^6$  represents the linear and angular velocity of the  $i^{th}$  IAB about its screw basis. In essence,  $\mathbf{r}_i \in \mathbb{R}^3$  with its rows are mapped to scalars by an appropriate choice of norm<sup>2</sup>. The contact between the head and the IABs is mapped by the Jacobian

$$\mathbf{J}_{c_i}(\xi_h, \xi_{iab_i}) = \begin{bmatrix} \mathbf{I} & \hat{\mathbf{w}}(r_{c_i}) \\ \mathbf{0} & \mathbf{I} \end{bmatrix} J_{r_i}, \quad (5)$$

where  $\mathbf{J}_{c_i} : \dot{\xi}_{r_i} \rightarrow [v_{c_i}^T, w_{c_i}^T]^T$ ,  $r_{c_i} \in \mathbb{R}^3$  is a vector between the head reference point (e.g. the center of mass) and the contact with the  $i^{th}$  IAB,  $\xi_h$  is the position and relative orientation of the head,  $\xi_{iab_i}$  is the position and relative orientation of the  $i^{th}$  soft robot in world coordinates,  $\hat{\mathbf{w}}(r_{c_i})$  is an anti-symmetric matrix for the vector  $r_{c_i}$ , and  $\xi_r = (\xi_{r_1}, \xi_{r_2}, \dots, \xi_{r_k})$ ,  $(1 \leq k \leq n)$  are the positions and orientations for each of the IABs. For  $C^2$ -smooth  $k$ -constraint functions  $G_1, \dots, G_k$  ( $1 \leq k \leq n$ ), a constraint is fulfilled when  $g_i(\xi) = 0$  and we write out the composite constraint function  $G : \mathbb{R}^n \rightarrow \mathbb{R}^k$  with respect to the contact Jacobians as

$$G_i^T(\xi_h, \xi_{iab_i}) \xi_h = B_i^T(\xi_h, \xi_{iab_i}) \mathbf{J}_{c_i}(\xi_h, \mathbf{r}_i) \dot{\xi}_{iab_i} \quad (6)$$

for an IAB's selection matrix  $B_i^T(\xi_h, \xi_{iab_i}) \in \mathbb{R}^{m_i}$ , where  $m_i$  is the range of all the forces and moments for the chosen contact primitive (or union of contact primitives). Therefore, for  $k$  actuators in the soft robot, we have the following manipulation constraint

$$\begin{bmatrix} G_1^T \\ \vdots \\ G_k^T \end{bmatrix} \begin{pmatrix} v_h \\ w_h \end{pmatrix} = \text{diag} \begin{pmatrix} B_1^T \mathbf{J}_{c_1} \\ \vdots \\ B_k^T \mathbf{J}_{c_k} \end{pmatrix} \begin{pmatrix} \dot{\mathbf{r}}_{iab_1} \\ \vdots \\ \dot{\mathbf{r}}_{iab_k} \end{pmatrix}. \quad (7)$$

The details of this derivation are presented in my unpublished work [28]. We call  $\mathcal{M}_{free}$  the free constraint manifold of the overall manifold,  $\mathcal{M}$ , which is defined as  $\mathcal{M}_{free} = \mathcal{M} \cap \mathcal{Q}_{free}$ .

**Problem 1** (Constrained RCLF Motion Planning). *Find an RCLF collision-free path  $\sigma^* : [0, 1] \rightarrow \mathcal{M}_{free}$  given a path planning problem  $(\mathcal{Q}_{free}, \xi_i, \mathcal{Q}_{goal})$ , manipulation constraint,  $G$ , and cost function  $V$  such that  $V(\sigma^*) = \min_{\sigma \in \Sigma_{\mathcal{M}_{free}}} V(\sigma)$  if one exists.*

**Expected results:** Previously, the stabilizing command for items 1 and 2 in subsection B above was computed by solving a constrained optimization problem to choose the collision-free stabilizing command among the possible solutions. My implementation takes a greedy approach using the L-BFGS optimization algorithm with box constraints, in contrast to the quadratic nonlinear constrained optimization used by [63], to find the minimal value of the control law  $u$  at each time step such that  $u$  is stable. Results of this implementation on toy robot nonlinear control from example demonstrations in 2D task space, implemented in python (see [64]), are reprinted in Fig. 10. When the problem identified in Prob. 1 is solved, I should expect my results to provide better trajectory tracking than the non-RCLF implementation I implemented in [64] owing to the account for all possible manifold constraints in the problem formulation.

### 3.3.3 $K_{99}$ Aim III: Mechanism Assembly. Phantom and Healthy Volunteer Experiments.

#### Rationale.

**Case for a parallel soft manipulator:** Open-loop kinematic chains have a low transportable load and poor accuracy since the weight of the segments that follow each link and the load of the structure contributes to the large flexure of torques; their links magnify errors from shoulder out to the end-effector, consequently hampering their use for sophisticated control strategies that may minimize or eliminate load-dependent error. Thus, most serially-joined manipulators are stiffened during the manufacturing process – thus, inherently exhibiting a high load-to-weight ratio and a complicated actuation system. Moreover, their passive bending stiffness overwhelms the degree of deformation. Parallel configurations, in spite of their higher number of actuated joints, distribute the weight of the load around the links of the robot, improve manipulation accuracy, have a desirable lightness property (albeit at the expense of a reduced workspace), and minimize the flexure torques that are otherwise common with open-loop kinematic chains. Given the non-cumulative nature of actuator errors in parallel configurations, greater precision is possible with minimal control-complication [65].

<sup>2</sup>I used the  $l_2$ -norm in my implementation.

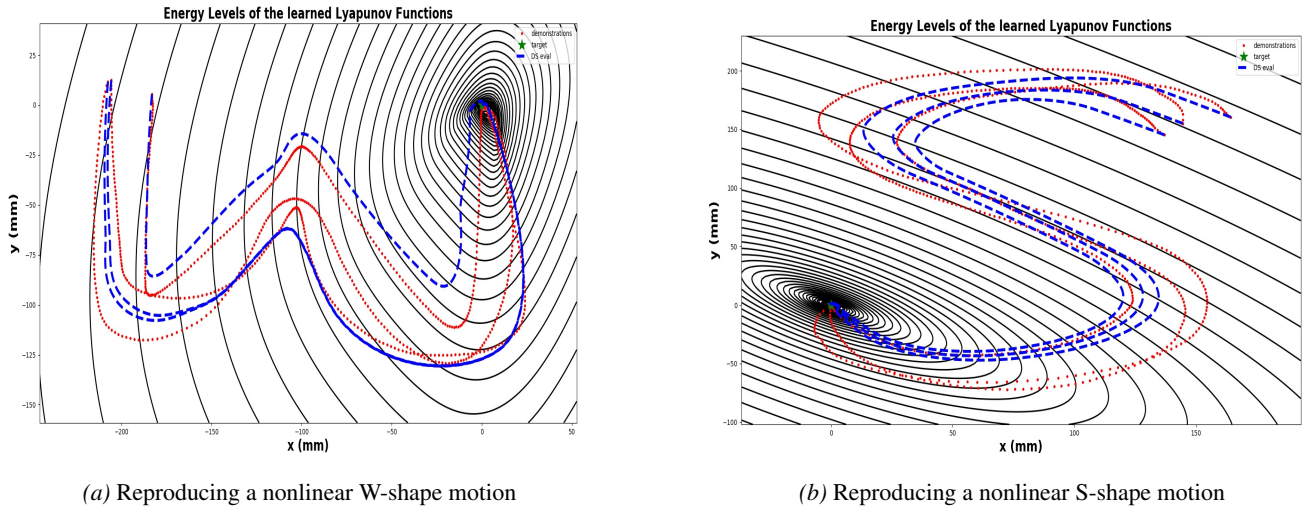


Figure 10: A CLF motion executor (red curves) that shows convergence to local attractors (green asterisks) and follows 3 different set trajectories (blue curves) for 2D nonlinear motion-trajectory problems on the WAM robot.

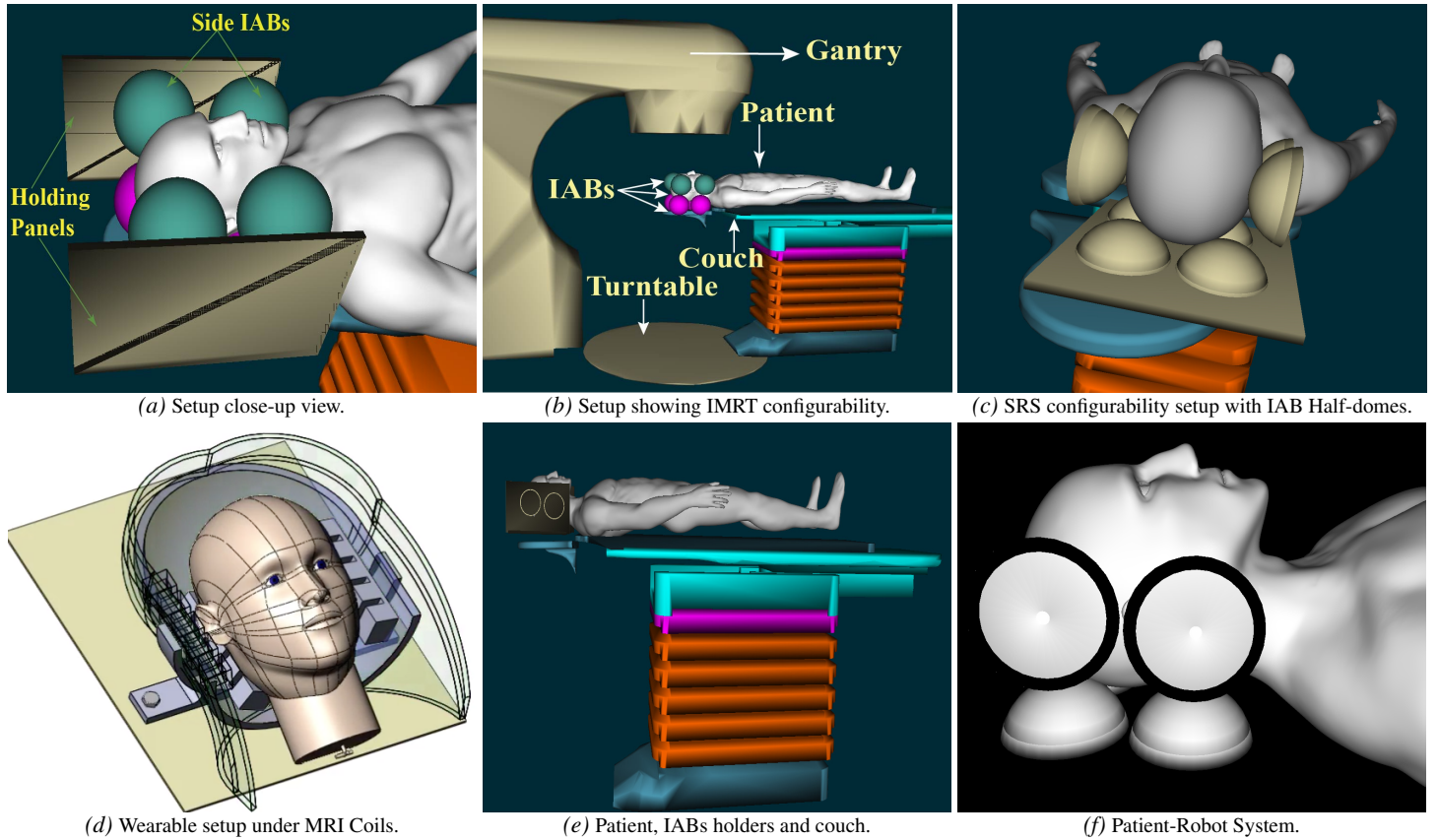


Figure 11: Proposed MRI-compatible LINAC patient motion compensation system.

### Hypothesis.

Owing to the success of parallel robot mechanisms at precise manipulation tasks [2, 20, 66–68], **I hypothesize that a parallel soft-manipulator mechanism will yield the desired submillimeter and subdegree accuracy necessary for online, real-time head motion control in MRI-LINAC RT.**

### Procedure.

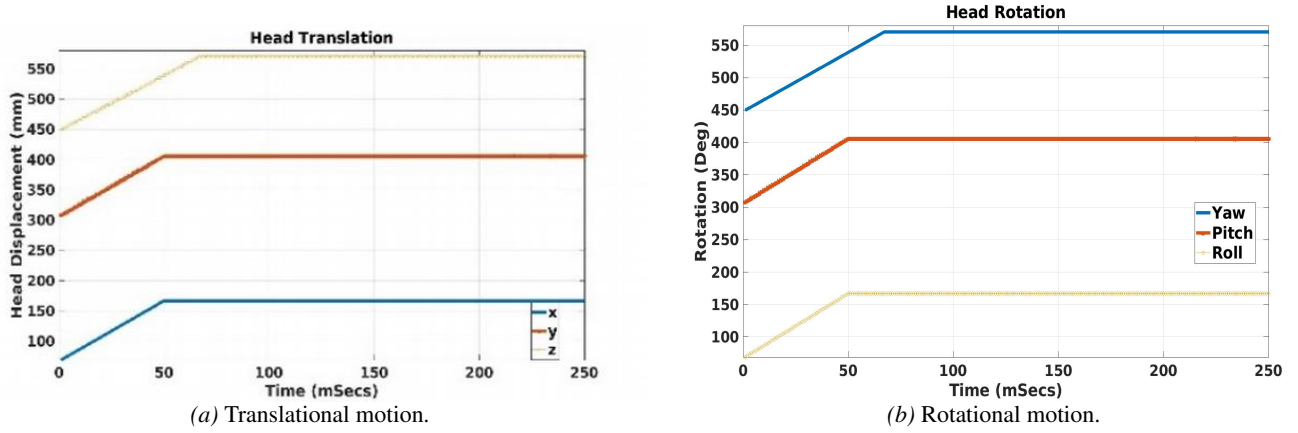


Figure 12: Open-loop setpoint-following for patient's head motion in  $\mathbb{SE}(3)$ . Reprinted from [13].

**A. Head Motion Correction in  $\mathbb{SE}(3)$ :** I will systematically synthesize and analyze parallel soft robot manipulators for head and neck motion correction in MRI-LINAC systems. I will then leverage the kinematics and kinetics of soft manipulators which I proposed in [28] to construct the hierarchical motion planner in Aim II. Synthesizing multi-DOF parallel soft robots is challenging given the inter-dependency of the parameters that characterize the deformation, the individual robot constraints' relative three dimensional orientation, permitted motion orientations, the three dimensional relation between constraints and allowed motions, and the possibility of multiple assembly modes that may result in the same end-effector pose [66]. The configuration that shall be investigated shall consist of soft actuators so arranged that their independent or coupled actuation can produce the needed head motion correction along the left-right (LR), the anterior-posterior (AP), and/or the superior-inferior (SI) axes. I will analyze the manipulation map, kinematics and kinetics of the respective closed-loop chains, and analyze the contact equations between the IAB system and head.

Fig. 11b shows an example standalone motion correction prototype for an IMRT system while Fig. 11c shows the proposed mechanism for MRI-LINAC systems (without MRI coils). Owing to the modular design, the coils of an MRI can be easily integrated onto this mechanism. In a parallel kinematic manner, the soft domes are positioned around the patient's cranial region while the patient lies supine on a typical MRI/RT treatment couch (Fig. 11b). The soft domes will be held in place around the head by impact-resistant low-temperature rigid PVC foam insulation sheet that is encased in carbon fiber. Velcro stickers (not shown) will be affixed to the planar soft dome holders to accommodate different patient cranial geometry – thus providing a modularization that ensures re-usability for different patients. The side actuators will correct head motion along the LR axis of the head anatomy *i.e.* (yaw and roll motions), while the bottom ones will correct head motion along the AP direction. The SI motion will be adjusted by the two lower actuators on the bottom of the neck. These will conform deformation in a non-Gaussian fashion through an appropriate configuration of fiber-reinforcing (see [videos](#)). The domes underneath the forehead would control pure  $z$  translation and pitch rotary motions.

In preliminary work [28], I have synthesized differential kinematics [69], continuum mechanics [70,71] and multi-bodied kinematics. Equation (7) yields the cranial manipulation constraint between the soft actuators and the head so that we can find the respective translational and rotational head velocity components,  $v_h, \omega_h$  respectively in world frames. We can easily find the pseudo inverse of the manipulation map,  $G$  in (7), so as to determine head velocity on the treatment couch. The derivation of this equation is detailed in [27].

**B. Expected Results:** I would expect that my results will follow the open-loop head motion control simulation results in the SOFA [72] framework as presented in my recently accepted publication [13] using the proposed setup of Fig. 11f: raising or rotating the head in  $\mathbb{SE}(3)$  resulted in steady-state reference trajectory tracking along all 6-DoFs of head motion as shown in Fig. 12.

### 3.3.4 $R_{00}$ Aim: Patient oncological clinical trials.

To verify accuracy of delivered dose, a complete end-to-end evaluation of the robotic MRI-compatible RT system will be conducted using anthropomorphic phantom studies. From the preliminary data (Fig. 3, 5, 12), whereupon excellent agreement was found between head motion and given target trajectory using the adaptive controller proposed in [20]. Once we ascertain the efficacy of this, we will move to healthy human volunteer trials.

**Statistical Plan:** Phantom-based and healthy human volunteer trials will be conducted after we finish the design and build of the proposed system. A complete end-to-end testing with 3D printed head phantoms containing dosimetric gel will be used to evaluate 3D radiation dose accuracy for both single and multiple target MRI-compatible RT plans. A 20 volunteer study with a mock radiation beam will be conducted in a clinical environment to verify 6DOF head control and patient safety systems. A clinical study on 20 whole brain patients will be performed where validation of method will be determined by a statistical endpoint defining success as to whether or not the 6D intracranial target is  $\leq 0.5\text{mm}$  and  $\leq 0.5^\circ$  for greater than 95% of the treatment time.